
Article:
Driscoll, P. and Davies, C. (2022) The “New Core Paradox”: Challenges and Potential Solutions. Journal of Geophysical Research: Solid Earth, 128 (1). e2022JB025355. ISSN: 2169-9313

https://doi.org/10.1029/2022JB025355

JGR Solid Earth

RESEARCH ARTICLE
10.1029/2022JB025355

The "New Core Paradox": Challenges and Potential Solutions

P. Driscoll[1] and **C. Davies**[2]

[1]Earth & Planets Lab, Carnegie Institution for Science, Washington, DC, USA, [2]School of Earth & Environment, University of Leeds, Leeds, UK

Key Points:

- Using nominal thermal evolution parameters the geodynamo is predicted to die prior to inner core nucleation
- Keeping it alive requires either a low thermal conductivity (20 W/m/K), a high core radioactivity (3 TW), or a hot initial core (6,000 K)
- A relatively low core melting temperature of 5,300 K correlates with higher ohmic dissipation prior to inner core nucleation

Correspondence to:
P. Driscoll,
pdriscoll@carnegiescience.edu

Citation:
Driscoll, P., & Davies, C. (2023). The "new core paradox": Challenges and potential solutions. *Journal of Geophysical Research: Solid Earth*, *128*, e2022JB025355. https://doi.org/10.1029/2022JB025355

Received 5 AUG 2022
Accepted 12 DEC 2022

Author Contributions:
Formal analysis: P. Driscoll
Software: P. Driscoll, C. Davies
Writing – original draft: P. Driscoll, C. Davies
Writing – review & editing: P. Driscoll, C. Davies

Abstract The "new core paradox" suggests that the persistence of the geomagnetic field over nearly all of Earth history is in conflict with the core being highly thermally conductive, which makes convection and dynamo action in the core much harder prior to the nucleation of the inner core. Here we revisit this issue by exploring the influence of six important parameters on core evolution: upper/lower mantle viscosity ratio, core thermal conductivity, core radiogenic heat rate, mantle radiogenic heating rate, central core melting temperature, and initial core-mantle boundary (CMB) temperature. Each parameter is systematically explored by the model, which couples mantle energy and core energy-entropy evolution. A model is "successful" if the correct present-day inner core size is achieved and the dynamo remains alive, as implied by the paleomagnetic record. In agreement with previous studies, we do not find successful thermal evolutions using nominal parameters, which includes a core thermal conductivity of 70 $Wm^{-1}K^{-1}$, zero core radioactivity, and an initial CMB temperature of 5,000 K. The dynamo can be kept alive by assuming an unrealistically low thermal conductivity of 20 $Wm^{-1}K^{-1}$ or an unrealistically high core radioactive heat flow of 3 TW at present-day, which are considered "unsuccessful" models. We identify a third scenario to keep the dynamo alive by assuming a hot initial CMB temperature of ∼6,000 K and a central core liquidus of ∼5,550 K. These temperatures are on the extreme end of typical estimates, but should not be ruled out and deserve further scrutiny.

Plain Language Summary The cooling of Earth over geological time is of interest to many scientific disciplines and has been studied intensively. Maintaining the geomagnetic field requires continuous core cooling to drive fluid motion in Earth's liquid iron outer core. Recent studies have shown that the materials that make up Earth's core can conduct heat very efficiently, which makes fluid motion in the core more difficult. In this study we investigate the thermal and magnetic evolution of Earth using a core-mantle cooling model. In particular, we investigate how several important aspects of Earth's interior that control its thermal and magnetic evolution over 4.5 billion years. In agreement with previous studies, we confirm that typical models fail to reproduce the thermal and magnetic evolution found in the geological record. We identify a potentially new solution that invokes (a) that the core is initially super hot following the formation of the Earth, and (b) that the melting temperature of the core material is lower than most estimates. This potential solution should be investigated further by studying the initial core temperature following planet formation and careful measurement of the melting temperatures of iron alloys.

1. Introduction

The "new core paradox" (Olson, 2013) suggests that the persistence of the geomagnetic field over nearly all of Earth history (Bono et al., 2022; Fu et al., 2021; Tarduno et al., 2020) is in conflict with the core being highly thermally conductive (Pozzo et al., 2022; Williams, 2018), which makes convection and dynamo action in the core much harder prior to the nucleation of the inner core. Older theoretical estimates of the thermal conductivity of high pressure iron around 30–50 $Wm^{-1}K^{-1}$ (Stacey & Anderson, 2001; Stacey & Loper, 2007), and supported by some recent studies (Basu et al., 2020; Hsieh et al., 2020; Konôpková et al., 2016; Saha et al., 2020), are in accordance with the geodynamo being at least in part thermally driven by a modest core-mantle boundary (CMB) heat flow of 3–10 TW. On the otherhand, higher values of the core thermal conductivity of 70–200 $Wm^{-1}K^{-1}$ have been found by many high pressure-temperature laboratory experiments and computations (de Koker et al., 2012; Gomi et al., 2013; Inoue et al., 2020; Li et al., 2021; Pozzo et al., 2012, 2022; Xu et al., 2018; Zhang et al., 2020, 2022). Such a high thermal conductivity implies that core convection driven by thermal cooling alone is less efficient, and that the modern-day geodynamo must rely heavily on the buoyancy provided by inner core growth. Given this conclusion, it becomes even harder to explain how the geodynamo was driven prior to inner core formation. Although the age of the inner core remains unknown, it is likely younger than the oldest

paleomagnetic evidence that supports the existence of a geodynamo going back 3–4 Ga (Bono et al., 2022; Fu et al., 2021; Tarduno et al., 2020), implying that the geodynamo was maintained by thermal convection prior to inner core nucleation in a highly conducting core.

In addition to the "new core paradox," an (historically) older and more menacing paradox lingers in the mantle: the so-called "thermal catastrophe." The "thermal catastrophe" is found by thermal history models that integrate the modern-day mantle and core states back in time, predicting impossibly hot temperatures only 2–3 Ga that are in direct conflict with several lines of evidence, including paleo-geothermal estimates of mantle temperature (Davies, 1980, 2009; Herzberg et al., 2010; Keller & Schoene, 2018; Korenaga, 2006). The thermal catastrophe, which is equally problematic for the thermal history of the core, is not new and has been debated for decades. Davies (1980) demonstrated that the thermal catastrophe can be avoided if the Urey ratio (fraction of surface heat flow coming from radiogenic heating) is about twice the geochemically preferred value of $Ur \approx 0.3$. Thermal history models are very sensitive to the magnitude and decay time of radiogenic heating, the temperature sensitivity of the mantle's rheology, and the modern-day surface heat flow. Recently, Patočka et al. (2020) concluded that backwards thermal history models with no core radioactivity could avoid a catastrophe by assuming very cold initial potential mantle temperatures. Small changes to any of these parameters can mean the difference between cold and hot solutions at 4.5 Ga.

Christensen (1985) demonstrated that variable viscosity convection models with a weaker dependence of surface heat flow on temperature ($Q \sim T^{\beta}$, $\beta = 0.1$) than classic isoviscous theory ($\beta = 1/3$) can lead to reasonable thermal histories with realistic Urey ratios. This solution, of a low value of β, was later reinterpreted to be caused, for example, by the work required to bend thick subducting plates (Conrad & Hager, 1999), or to increased lithospheric thickness at high temperatures caused by extensive melting (Korenaga, 2006). Although recent models claim that plate bending does not dominate the dissipation (Gerardi et al., 2019), these issues remain somewhat unsettled.

In fact, problems with the core energy and entropy budgets predate the recent upward revisions to thermal conductivity. Obtaining a successful thermal evolution that does not invoke core radioactivity is problematic even when adopting the lower end of the thermal conductivity values (Driscoll & Bercovici, 2014; Gubbins et al., 2003, 2004; Nimmo et al., 2004). Proposed solutions include a colder core solidus, a shallower core adiabat, or a slower core cooling rate than expected (Nimmo et al., 2004). Additionally, the problem can be somewhat mitigated if the core is thermally convective beneath a stably stratified layer (Greenwood et al., 2021; Helffrich & Kaneshima, 2010; Labrosse, 2015), although dynamo simulations with imposed stratified layers favor models with relatively thin layers (Christensen, 2018; Gastine et al., 2020; Olson et al., 2017). Exsolution of a minor species from the core has the potential to drive compositional convection without inner core growth (Badro et al., 2018; Hirose et al., 2017; Mittal et al., 2020; O'Rourke & Stevenson, 2016). However, the core must cool relatively quickly for the exosolution-driven buoyancy to overcome any thermal stratification (Du et al., 2017, 2019) and the core may not contain enough lithophile elements to produce any exsolution (Chidester et al., 2022). Flows driven by precession are thought to be too weak to generate strong magnetic fields (Landeau et al., 2022).

Although this paper focuses on demonstrating the new core paradox, it will become apparent that these two problems with the evolution of the Earth are intertwined. In fact, a milder formulation of the new core problem predates the recent experiments, as stated by Davies (2007): "In the present case, it has seemed to be not possible simultaneously to reconcile the energy requirements of the geodynamo, the evidence for a magnetic field through most of Earth's history, the present size of the inner core and geochemical and cosmochemical constraints on the potassium content of the Earth." In other words, the thermal catastrophe is a major problem for the history of the core, and it is exaggerated by upward revisions to the core thermal conductivity.

In this paper we address these important issues by coupling together two existing thermal evolution codes, the whole-planet thermal evolution model from Driscoll and Bercovici (2014) with the core entropy evolution model from Davies (2015), to investigate how several important parameters influence the calculated thermal and magnetic evolutions. The parameters we explore are the core melting temperature, core thermal conductivity, core and mantle radiogenic heating rate, mantle viscosity, and initial core temperature. These are classic thermal evolution models in the sense that they do not include exotic mechanisms, like exsolution, stable

layers, a basal magma ocean (BMO), or chemical interactions with the mantle. "Successful" models are those that achieve the seismically inferred present-day inner core radius of 1,221 km, and that predict an operative geodynamo prior to inner core nucleation and at the present-day. Our goal here is to investigate the severity of the new core paradox, identify if any parameter regimes can resolve the problem, and provide motivation for future avenues of research.

2. Model

To calculate the coupled energy-entropy evolution of Earth's core a thermal (energy) evolution of the mantle, based on the model from Driscoll and Bercovici (2014) (referred to as DB14), is coupled to the core entropy evolution model, from Davies (2015) (referred to as D15). DB14 solves the mantle energy balance,

$$Q_{surf} = Q_{m,rad} + Q_{cmb} + Q_{\mathrm{sec},man} \tag{1}$$

where Q_{surf} is the mantle surface heat flow, $Q_{m,rad}$ is mantle radioactivity, Q_{cmb} is CMB heat flow, and $Q_{\mathrm{sec},man} = -M_m c_m \dot{T}_m$ is the mantle secular cooling heat loss, where M_m, c_m, and $\dot{T}_m$ are the mantle mass, specific heat, and rate of change of mantle temperature T_m. Q_{surf} and Q_{cmb} are functions of mantle and core temperatures (see Appendix A and DB14 for details). Parameters of the mantle model that are the same for all models include the following: a mobile lid Nu-Ra scaling law to relate mantle temperature to surface heat flow with a boundary layer theory exponent of $\beta = 1/3$, a temperature-dependent upper mantle (UM) viscosity that is calibrated to give the measured present-day mantle heat flow of 39 TW for the present-day mantle potential temperature of 1630 K (see Table 3 in DB14 for details), and no eruptive mantle cooling.

The core model, the same as used in D15, solves the core energy Q and entropy E balances,

$$Q_{cmb} = Q_{\mathrm{sec},core} + Q_L + Q_g + Q_{c,rad} \tag{2}$$

$$E_J + E_k + E_a = E_{\mathrm{sec},core} + E_L + E_g + E_h + E_{c,rad} \tag{3}$$

where subscripts are sec, *core* for secular cooling, L for latent heat, g for gravitational energy/entropy, *rad*, c for core radiogenic heating, and E_J is Ohmic dissipation, E_k is the entropy of thermal conduction, E_a is the entropy of molecular diffusion of minor species, and E_h is the entropy of reaction. Contributions due to pressure heating and pressure release upon freezing are considered to be negligible and are not considered. All entropy terms except E_J are written in terms of core thermodynamic properties and solved as the core cools (for details see D15). Our criteria to drive a dynamo is that there must be excess entropy available so that $E_J > 0$, otherwise the dynamo cannot operate. We note that E_J is an integration over the entire outer core, and we do not account for potential stratified layers within the outer core, which is not expected to change the results significantly (Greenwood et al., 2021).

The DB14 mantle energy and D15 core entropy models are coupled by an iterative procedure as follows:

1. The CMB temperature $T_{cmb}(t)$ and heat flow $Q_{cmb}(t)$ at a time t are determined by the DB14 model and input to the D15 model.
2. The D15 model then computes the entropy balance in Equation 3, the inner core radius $R_{ic}(T)$, and core cooling rate $\dot{T}_c(t)$.
3. The DB14 model then reads in these values and iterates to the next time step in the mantle and core, providing an updated value of T_{cmb} and Q_{cmb}.

This iterative procedure continues until $t = 4.5$ Gyr.

With the coupled models we explore six important and uncertain control parameters:

1. The CMB core thermal conductivity k,
2. The modern day core radiogenic heat production rate $Q_{c,rad}$ (assumed to be ^{40}K),
3. The modern day mantle radiogenic heat production rate $Q_{m,rad}$,
4. The core iron alloy liquidus defined at the center of the Earth $T_{melt,cen}$ (or equivalently CMB liquidus temperature $T_{melt,cmb}$),

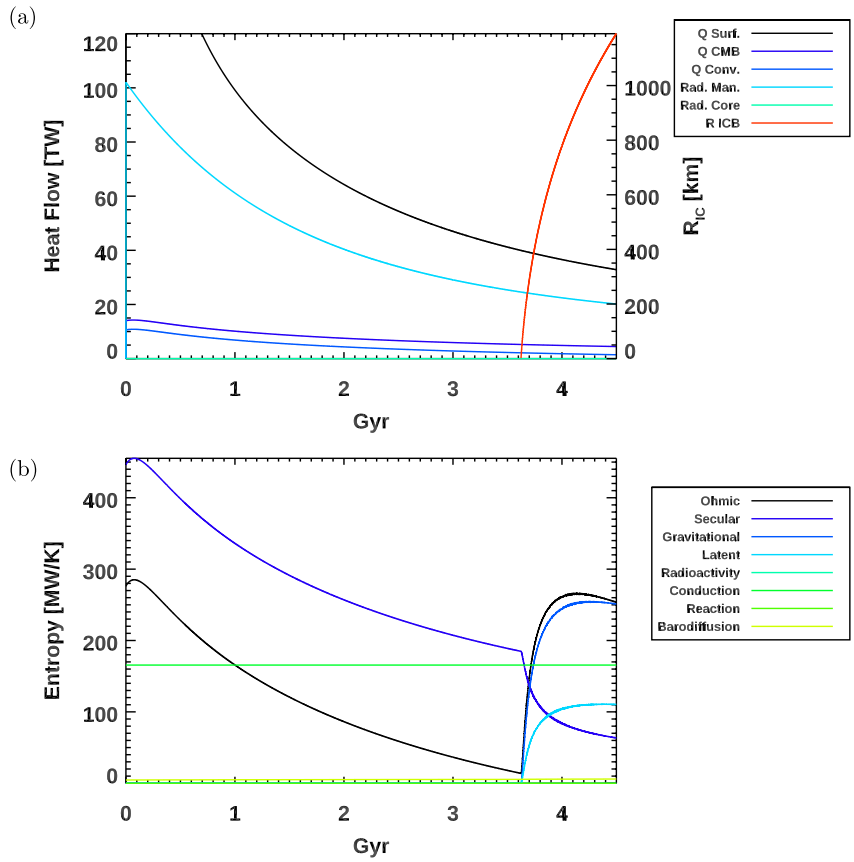

Figure 1. A "classical" thermal evolution model with a low core-mantle boundary (CMB) thermal conductivity of $k = 20$ Wm^{-1}K^{-1}, mantle viscosity ratio of $f_\nu = 70$, central core melting temperature of $T_{melt,cen} = 5{,}800$ K, initial core temperature of $T_{c,0} = 6{,}000$ K ($T_{cmb,0} = 4{,}570$ K), and zero core radioactivity $Q_{c,rad} = 0$ TW. (a) Heat flows at the surface, at the CMB, at the CMB minus core adiabat (i.e., core convective), at the inner core boundary, and mantle and core radioactive heating. The inner core nucleates at 875 Ma. Inner core radius R_{IC} (red) is shown on right y-axis. (b) Entropy evolution of the same model.

5. The initial CMB temperature $T_{cmb,0}$ (or equivalently initial average core temperature $T_{c,0}$),
6. And the ratio of the lower mantle (LM) to UM viscosity $f_\nu = \nu_{LM}/\nu_{UM}$.

Models are considered to be "successful" if they achieve the seismically inferred present-day inner core radius of 1,221 km at the present-day, and that find a positive ohmic dissipation prior to inner core nucleation and at the present-day. In the next section we will demonstrate how each of these control parameters influences the thermal and magnetic evolution.

One caveat with this model is that it does not account for melting of the deep mantle, which is expected to occur in the cases with hot initial cores. The effect of a BMO on core cooling is unsettled, with some predicting an insulating effect (Andrault et al., 2016; Labrosse et al., 2007; Laneuville et al., 2018; Monteux et al., 2016) and others predicting faster cooling (Agrusta et al., 2020; Labrosse et al., 2018). Adding the physics and composition of the BMO requires the addition of a number of poorly determined parameters. We prefer to keep a simpler model with fewer free parameters, while acknowledging that it is potentially important.

3. Results

3.1. "Classical" Solution

Before demonstrating the new core paradox, we first show an example of a thermal history solution with a classical low core thermal conductivity of $k = 20$ Wm^{-1}K^{-1}. With such a low conductivity it is fairly easy

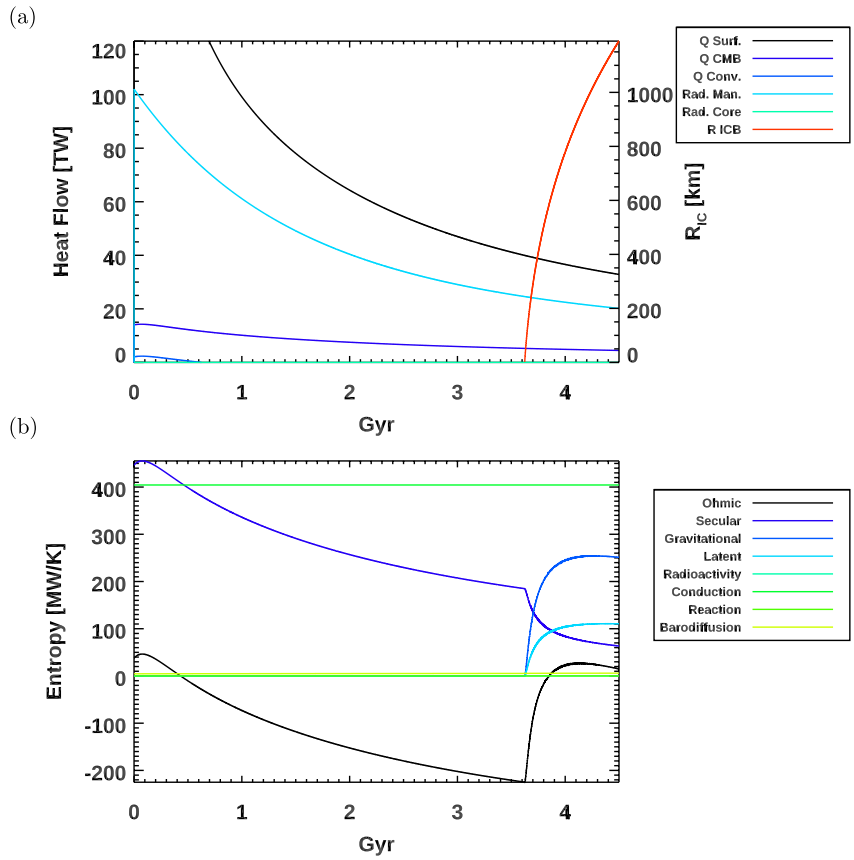

Figure 2. A thermal evolution model that demonstrates the new core paradox with a realistic core-mantle boundary (CMB) thermal conductivity of $k = 70$ Wm^{-1}K^{-1} and other parameters the same as Figure 1. (a) Heat flows at the surface, at the CMB, at the CMB minus core adiabat (i.e., core convective), at the inner core boundary, and mantle and core radioactive heating. The inner core nucleates at 875 Ma. Inner core radius R_{IC} (red) is shown on right y-axis. (b) Entropy evolution of the same model. Shaded region denotes period when $E_J < 0$ and there is no dynamo.

to produce solutions where the dynamo is alive for 4.5 Gyr (Figure 1). To ensure that the modern day inner core radius is achieved the other free model parameters are adjusted to a mantle viscosity ratio of $f_\nu = 70$, iron alloy melting temperature at the center of the Earth of $T_{melt,cen} = 5{,}800$ K, initial core temperature of $T_{c,0} = 6{,}000$ K ($T_{cmb,0} = 4{,}570$ K), and no core radioactivity $Q_{c,rad} = 0$ TW. Although this solution is not unique in producing the correct R_{IC}, it demonstrates how a low k value can produce a solution that maintains the dynamo over all of Earth history. However, this classical solution is not satisfactory because most recent experiments indicate the core thermal conductivity is likely 3–4 times larger than 20 Wm^{-1}K^{-1} (Pozzo et al., 2022).

3.2. Demonstrating the New Core Paradox

Next, we demonstrate the new core paradox (Figure 2) by increasing the thermal conductivity at the CMB to $k = 70$ Wm^{-1}K^{-1}, which is consistent with recent estimates (Pozzo et al., 2022), while keeping all other parameters the same as the classical solution in Figure 1. In this "failed" thermal history solution the inner core size is the same as the classical solution (Figure 2a) because the core thermal conductivity does not influence the cooling rate under our assumption of the outer core being well-mixed. In reality the core cooling rate could depend on the core thermal conductivity if it is thermally stratified, but this is not expected to be a significant effect (Greenwood et al., 2021). In this case E_J, and hence the dynamo, are subcritical from 0.4 to 3.9 Gyr (Figure 2). Over that period the core cooling and inner core growth rates are insuffi-

Table 1
Nominal Parameter Values and Nominal Ranges Used in the Energy-Entropy Model Parameter Sweeps

Parameter	Nominal value	Nominal range	Hot core solution
Core thermal conductivity, k ($Wm^{-1}K^{-1}$)	70	10–200	70
Mantle viscosity ratio, f_ν (n.d.)	70	1–100	5
Present-day core radiogenic heating rate, $Q_{c,rad}$ (TW)	0	0–5	0
Present-day mantle radiogenic heating rate, $Q_{m,rad}$ (TW)	13	12–30	13
Central core melting temperature, $T_{melt,cen}$ (K)	5,800	5,400–6,200	5,545
Initial CMB temperature, $T_{cmb,0}$ (K)	4,570	4,570–6,400	6,015

Note. The last column is the hot core solution shown in Figure 10. Note n.d. denotes non-dimensional. The nominal and range of central core melting temperatures ($T_{melt,cen}$) above correspond to present-day inner core boundary melting temperatures ($T_{melt,icb}$) of 5,500 K and 5,100–5,900 K, respectively. The nominal and range of initial core-mantle boundary temperatures ($T_{cmb,0}$) above correspond to initial average core temperatures ($T_{c,0}$) of 5,784–8100 K, respectively.

cient to overcome thermal conduction so the core is stably stratified, and no dynamo can operate. Shortly after inner core nucleation, however, compositional entropy production is sufficient to bring the dynamo back. The reason this model also "fails" is that there are many paleomagnetic observations during the 0.4–3.9 Gyr period that indicate the geodynamo was alive and well (Biggin et al., 2020; Bono et al., 2022; Fu et al., 2021; Tarduno et al., 2020; Tauxe & Yamazaki, 2015).

3.3. Parameter Sweeps

Next, we systematically explore how six important control parameters (f_ν, k, $Q_{c,rad}$, $Q_{m,rad}$, $T_{melt,cen}$, and $T_{cmb,0}$) influence the thermal history. Parameter sweeps are performed over the following parameter values (see Table 1): 21 values of mantle viscosity ratio f_ν over the range 1–100, 20 values of thermal conductivity at the top of the core k over the range 10–200 $Wm^{-1}K^{-1}$, 21 values of present-day core radioactivity $Q^*_{c,rad}$ over the range 0–5 TW, 17 values of central core melting temperature $T_{melt,cen}$ over the range 5,400–6,200 K (equivalent to $T_{melt,ICB}$ = 5,100–5,900 K), and 11 values of initial CMB temperatures $T_{cmb,0}$ over the range 4,570–6,400 K (corresponding to initial average core temperatures $T_{c,0}$ over the range 6,000–8,000 K). The nominal values of these control parameters are (Table 1): k = 70 $Wm^{-1}K^{-1}$, $Q_{c,rad}$ = 0 TW, $Q_{m,rad}$ = 13 TW, $T_{melt,cen}$ = 5,800 K, and $T_{cmb,0}$ = 4,570 ($T_{c,0}$ = 6,000 K).

The range of values explored for each parameter is somewhat arbitrary, and in some cases we allow a wider range of values than is expected to gain a broader perspective on the thermal evolution problems. The viscosity increase across the mantle is uncertain, particularly in the lowermost mantle, with factors of 10–100 times increase of viscosity from the upper to LM proposed (Deng & Lee, 2017; Marquardt & Miyagi, 2015). We adopt a wide range of core thermal conductivities that reflects the values inferred by experiments and ab initio calculations (Hsieh et al., 2020; Konôpková et al., 2016), with the unknown composition of light elements in the core adding to the uncertainty. Heat produced by radiogenic decay in the core is typically inferred to be small compared to the CMB heat flow, mainly due to the lithophilic nature of the main radiogenic species in Earth (Blanchard et al., 2017; Bouhifd et al., 2007; Chidester et al., 2017; Corgne et al., 2007; Faure et al., 2020; Hirao et al., 2006; Watanabe et al., 2014; Xiong et al., 2018). However, some authors find a modest amount of radioactivity remains possible (Adeleke & Yao, 2020; Chidester et al., 2022; Wohlers & Wood, 2015). The core solidus at the inner core boundary (ICB) is uncertain, with estimates ranging from 5,000 to 7,000 K (Hirose et al., 2021). The initial temperature of the core is somewhat constrained by the partitioning of elements during core-mantle separation, implying equilibration temperatures at least 300–500 K above the silicate liquidus (Fischer et al., 2017), corresponding to 4,800–5,000 K at the CMB, but could have been much hotter.

3.3.1. Influence of Core Thermal Conductivity

A parameter sweep of core thermal conductivity k and mantle viscosity ratio f_ν is shown in Figure 3, with all other parameters set to their nominal values (Table 1). The panels are contours of final inner core radius R_{IC}

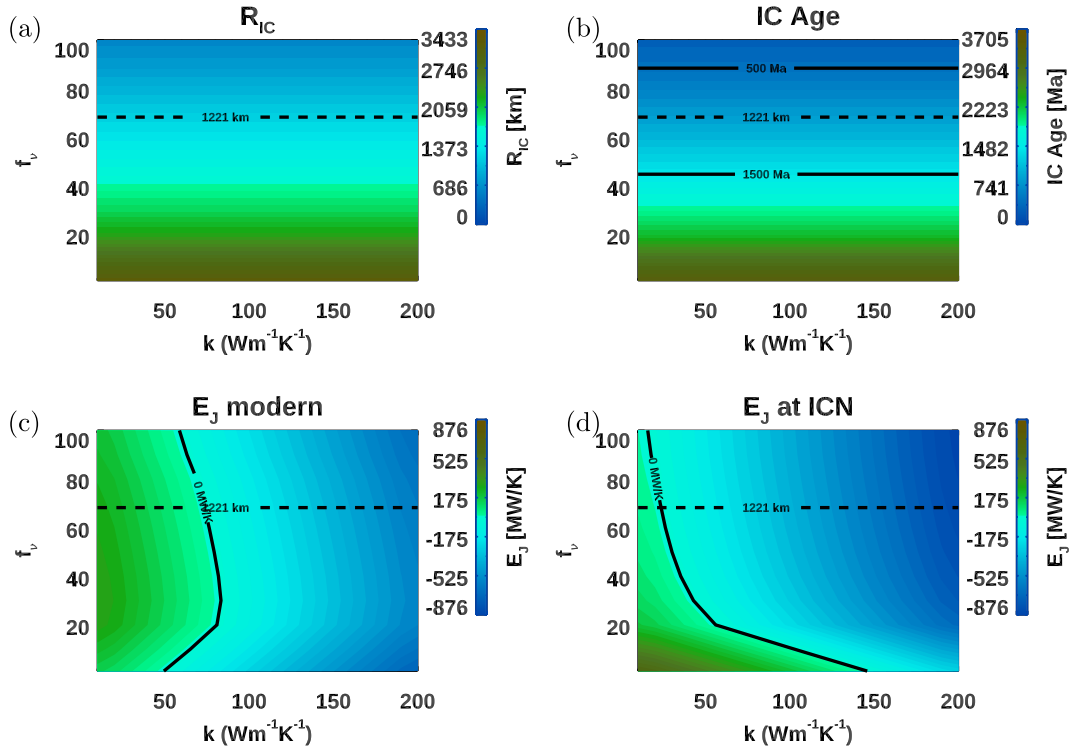

Figure 3. A parameter sweep over core-mantle boundary thermal conductivity k and mantle viscosity ratio f_ν. Other control parameters are fixed to their nominal values: $Q_{c,rad} = 0$ TW, $Q_{m,rad} = 13$ TW, $T_{melt,cen} = 5{,}800$ K, and $T_{cmb,0} = 4{,}570$ K. Contours of final inner core radius R_{IC} (a), age of inner core nucleation (b), core ohmic dissipation at the present-day E_J(4.5 Gyr) (c), and ohmic dissipation at inner core nucleation E_J(ICN) (d). In all contours Earth's present-day inner core radius $R_{IC} = 1{,}221$ km is shown as a dashed black curve. Solid black lines denote inner core ages of 500 and 1,000 Ma in (b), and denote ohmic dissipation contours of 0 and −200 MW/K in (c) and (d).

(Figure 3a), inner core age (Figure 3b), final ohmic dissipation E_J (Figure 3c), and ohmic dissipation at inner core nucleation (Figure 3d). Inner core radius and age does not depend on k (Figures 3a and 3b) because the core thermal conductivity does not effect the bulk core cooling rate in our model. Therefore, $R_{IC} = 1{,}221$ km constrains mantle viscosity ratio to $f_\nu \approx 70$ in this parameter space (dashed line in Figure 3). Given that $f_\nu \approx 70$ for $Q_{c,rad} = 0$, Figures 3c and 3d then imply that $k \lesssim 30$ Wm^{-1}K^{-1} to have a successful solution with $E_J > 0$ prior to inner core nucleation (ICN) and at present-day. These low k solutions are similar to the classical model in Figure 1, but are not satisfactory because k is likely larger than 30 Wm^{-1}K^{-1}, and they produce values of Q_{surf} that are several TW lower than the inferred present-day value of 39 TW (Jaupart et al., 2015).

3.3.2. Influence of Core Radioactivity

A parameter sweep of present-day core radioactive heat production $Q_{c,rad}$ (assumed to be produced entirely by the decay of ^{40}K) and mantle viscosity ratio f_ν is shown in Figure 4, with all other parameters set to their nominal values (Table 1). The constraint that the final inner core radius be $R_{IC} = 1{,}221$ km restricts f_ν and $Q_{c,rad}$ along a curve (dashed black in Figure 4). This curve is in the upper left of Figure 4 because the mantle viscosity must be relatively high ($f_\nu \sim 70$) when there is no core radioactivity ($Q_{c,rad} \sim 0$ TW) to prevent the core from cooling too fast and growing the IC too large. Conversely, the curve bends down to the lower right of Figure 4 because for high core radioactivity ($Q_{c,rad} \sim 3$ TW) the mantle viscosity must be relatively low ($f_\nu \sim 5$) to allow the core to cool enough to grow the IC to its present-day size. IC age is strongly correlated with R_{IC}, meaning that IC age is constrained around 500–1,500 Ma (Figure 4b). In addition to the R_{IC} constraint, finding a successful solution that maintains a dynamo both at present-day and prior to ICN requires that $Q_{c,rad} \gtrsim 2$ TW and $f_\nu \lesssim 10$ (bottom right of Figures 4c and 4d).

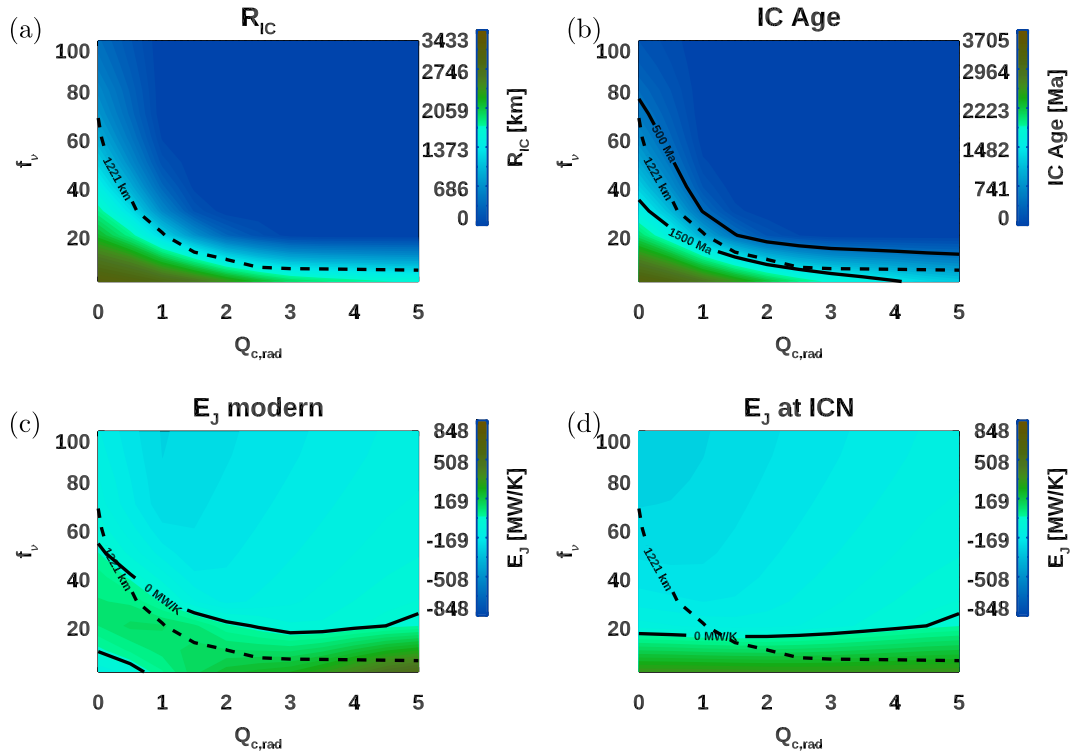

Figure 4. A parameter sweep of present-day core radioactivity $Q_{c,rad}$ and mantle viscosity ratio f_ν. Other control parameters are fixed to their nominal values: $k = 70$ Wm^{-1}K^{-1}, $Q_{m,rad} = 13$ TW, $T_{melt,cen} = 5{,}800$ K, and $T_{cmb,0} = 4{,}570$ K. Contours of final inner core radius R_{IC} (a), age of inner core nucleation (b), core ohmic dissipation at the present-day E_J(4.5 Gyr) (c), and ohmic dissipation at inner core nucleation E_J(ICN) (d). In all contours Earth's present-day inner core radius $R_{IC} = 1{,}221$ km is shown as a dashed black curve.

Contours of heat flows from the same models as in Figure 4 are shown in Figure 5. Figures 5a and 5b show that the mantle surface heat flow Q_{surf} and CMB heat flow increase with increasing $Q_{c,rad}$ and decreasing f_ν. Figures 5c and 5d show that the convective core heat flow ($Q_{conv} = Q_{cmb} - Q_k$, where Q_k is core conductive heat flow) is only positive prior to ICN and at present-day if $Q_{c,rad} \gtrsim 4$ TW and $f_\nu \lesssim 5$, consistent with the results in Driscoll and Bercovici (2014). Although there are some minor differences between the successful solutions spaces computed by the entropy balance (Figures 4c and 4d) and the energy balance (Figures 5c and 5d), they generally agree that $Q_{c,rad} \gtrsim 2.5$ TW and $f_\nu \lesssim 5$ to meet the constraints of present-day inner core size and continuous core convection with the other parameters set to their nominal values.

The present-day mantle surface heat flow, estimated to be $Q_{surf} \simeq 38$ TW (Jaupart et al., 2015), is produced by models with $Q_{c,rad} > 4$ TW and $f_\nu < 5$ (Figure 5a). This demonstrates that the combined mantle and core constraints can be satisfied over a common set of parameters ($Q_{c,rad} \gtrsim 3$ TW and $f_\nu < 5$), a conclusion also reached by previous studies (Driscoll & Bercovici, 2014; Patočka et al., 2020).

3.3.3. Influence of Mantle Radioactivity

The present-day radiogenic heating rate of Earth's mantle (excluding the continental crust) $Q_{m,rad}$ remains somewhat uncertain, with most estimates in the 10–20 TW range (Gando et al., 2011; Sammon & McDonough, 2022). Previous thermal evolution studies have demonstrated that large values of $Q_{m,rad} \simeq 20$ TW can resolve the thermal catastrophe of the mantle (Christensen, 1985; Davies, 2009; Driscoll & Bercovici, 2014), but geochemical evidence implies lower values of $Q_{m,rad} \simeq 13$ TW (Arevalo et al., 2009; Boyet & Carlson, 2006; Jaupart et al., 2015). Given its relatively large uncertainty, we adopt a plausible range of $Q_{m,rad} = 10$–25 TW.

A parameter sweep of the present-day mantle radioactive heat production $Q_{m,rad}$ and mantle viscosity ratio f_ν is shown in Figure 6, with all other parameters set to their nominal values (Table 1). Figure 6 shows that mantle

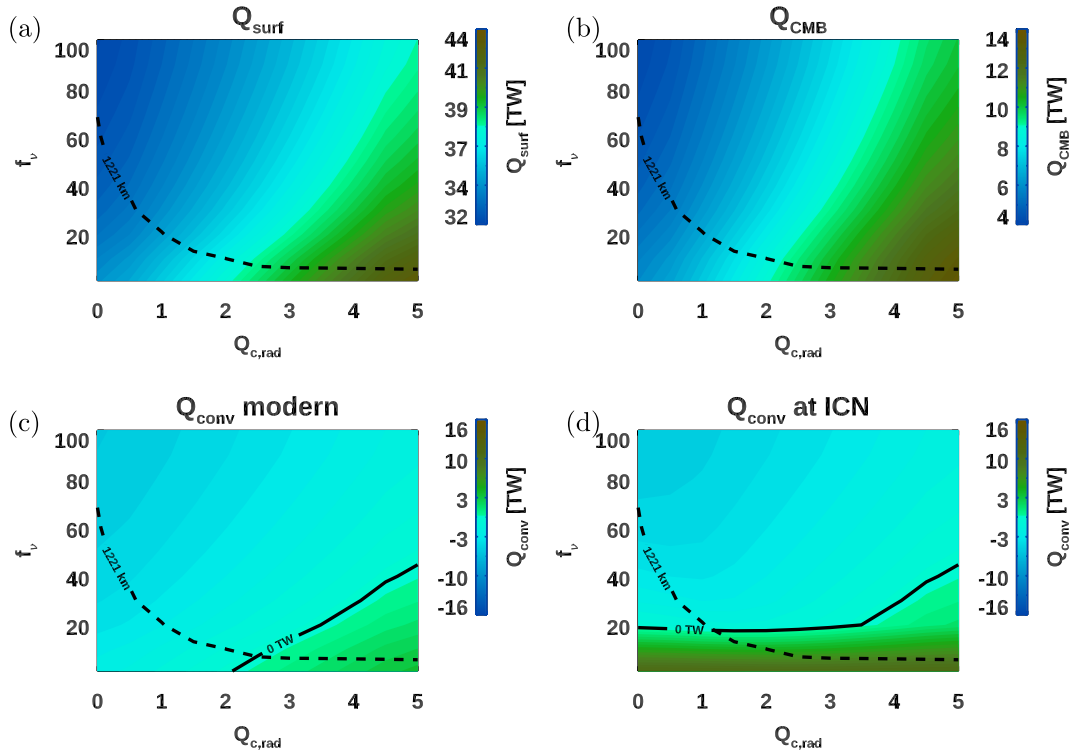

Figure 5. A parameter sweep over present-day core radioactivity $Q_{c,rad}$ and mantle viscosity ratio f_ν, similar to Figure 4. Other control parameters are fixed to their nominal values: $k = 70$ Wm^{-1}K^{-1}, $Q_{m,rad} = 13$ TW, $T_{melt,cen} = 5{,}800$ K, and $T_{cmb,0} = 4570$ K. Contours of final mantle surface heat flow Q_{surf} (a), final core-mantle boundary heat flow Q_{CMB} (b), final core convective heat flux ($Q_{conv} = Q_{CMB} - Q_{cond}$) (c), and Q_{conv} at inner core nucleation (d). In all contours Earth's present-day inner core radius $R_{IC} = 1{,}221$ km is shown as a dashed black curve and heat flow equal to zero is marked by a solid black curve.

radioactivity has a weaker influence on R_{IC} and the core cooling rate than core radioactivity (Figure 4). This is because at higher $Q_{m,rad}$ the mantle tends to remain hotter longer, which decreases the viscosity in the LM, leaving the core cooling rate largely unchanged. This implies that ohmic dissipation prior to ICN also does not depend strongly on $Q_{m,rad}$, and solutions with the correct final R_{IC} are firmly in the no-dynamo regime (Figure 6d). Therefore, unlike increasing $Q_{c,rad}$ above its nominal value, increasing $Q_{m,rad}$ alone does not help resolve the new core paradox.

3.3.4. Influence of Core Melting Temperature

A parameter sweep of central core melting temperature $T_{melt,cen}$ and mantle viscosity ratio f_ν is shown in Figure 7, with all other parameters set to their nominal values (Table 1). The correct R_{IC} can be achieved at low $T_{melt,cen}$ with a low value of f_ν that allows the core to cool fast, or a high $T_{melt,cen}$ with a high value of f_ν that reduces the core cooling rate (Figure 7a). IC age is again constrained between 500–1,500 Ma (Figure 7b), similar to Figure 4b. No successful dynamo solutions can be found in this parameter space as there are no regions where $E_J > 0$ prior to ICN and at present-day with the correct R_{IC} (Figures 7c and 7d). However, Figure 7d shows a near-successful solution is found around $f_\nu = 10$, $T_{melt,cen} = 5{,}400$ K, where the dashed contour (corresponding to correct IC size) nearly intersects the solid black contour (corresponding to an active dynamo at ICN).

3.3.5. Influence of Initial Core Temperature

Finally, a parameter sweep of initial CMB temperature $T_{cmb,0}$ and mantle viscosity ratio f_ν is shown in Figure 8, with all other parameters set to their nominal values (Table 1). Increasing initial core temperature has a similar effect as increasing core radioactivity (Figure 4): hotter values of $T_{cmb,0}$ require lower values of f_ν to meet the R_{IC} constraint (Figure 8a). Similar to Figure 4b, IC age is constrained between 500–1,500 Ma (Figure 8b), and a

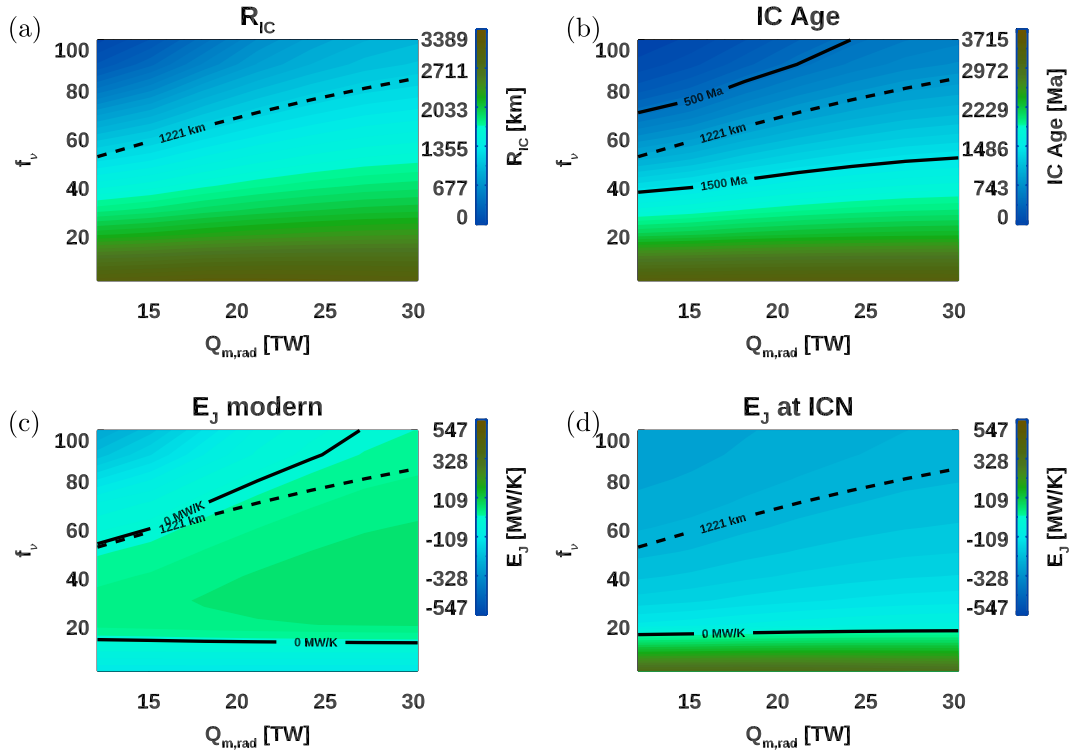

Figure 6. A parameter sweep over present-day mantle radioactivity $Q_{rad,man}$ and mantle viscosity ratio f_ν, similar to Figure 4. Other control parameters are fixed to their nominal values: $k = 70$ Wm^{-1}K^{-1}, $Q_{c,rad} = 0$ TW, $T_{melt,cen} = 5{,}800$ K, and $T_{cmb,0} = 4{,}570$ K. Contours of final mantle surface heat flow Q_{surf} (a), final core-mantle boundary heat flow Q_{CMB} (b), final core convective heat flux ($Q_{conv} = Q_{CMB} - Q_{cond}$) (c), and Q_{conv} at inner core nucleation (d). In all contours Earth's present-day inner core radius $R_{IC} = 1{,}221$ km is shown as a dashed black curve and heat flow equal to zero is marked by a solid black curve.

successful solution can be found in this parameter space as the $R_{IC} = 1{,}221$ km solutions (dashed line) do intersect both of the active dynamo regions of $E_J > 0$ prior to ICN and at present-day for initial CMB temperatures of $T_{cmb,0} \gtrsim 5{,}400$ K (Figures 8c and 8d). In this case, as $T_{cmb,0}$ increases solutions with $R_{IC} = 1{,}221$ km cross the E_J(ICN) = 0 contour (Figure 8d) because hotter initial cores take longer to cool down, and maintain a relatively high Q_{cmb} (and E_J) longer.

To investigate this potential solution further we repeat the parameter sweep from Figure 8 up to hotter initial core temperatures, $T_{cmb,0}$, and fix the central melting temperature to $T_{melt,cen} = 5{,}545$ K, which is the value of $T_{melt,cen}$ that yielded the closest solutions in Figure 7d. Figure 9 shows that this combination of parameters does indeed produce a range of "successful" solutions for $T_{cmb,0} \gtrsim 5{,}400$ K and $f_\nu < 5$ where solutions with the correct IC size intersect the active dynamo region (E_J(ICN) = 0 contour), implying continuous dynamo action. This interesting solution, which uses $k = 70$ Wm^{-1}K^{-1}, $f_\nu = 5$, $T_{cmb,0} = 6015$ K, $T_{melt,cen} = 5545$ K ($T_{melt,330\text{GPa}} = 5250$ K), $Q_{c,rad} = 0$ TW, and $Q_{m,rad} = 13$ TW, is isolated in Figure 10 as a time evolution. In this solution, E_J approaches zero around ICN at 627 Ma, and then recovers rather quickly due to gravitational entropy production associated with inner core solidification. This solution is "successful" in the sense that it keeps the dynamo alive, produces the correct final IC radius, and assumes zero core radioactivity, but it requires two rather unconventional temperatures: a hot initial CMB temperature of ~6,000 K, and a low core melting temperature of ~5,550 K at the center of the core. Nevertheless, this solution appears more plausible than the other options; namely those that assume significant core radioactivity (~3 TW) or a very low core conductivity (~20 Wm^{-1}K^{-1}). Invoking such a hot initial core has been suggested by previous studies (Labrosse, 2015; Nimmo, 2015), and is worthy of further investigation.

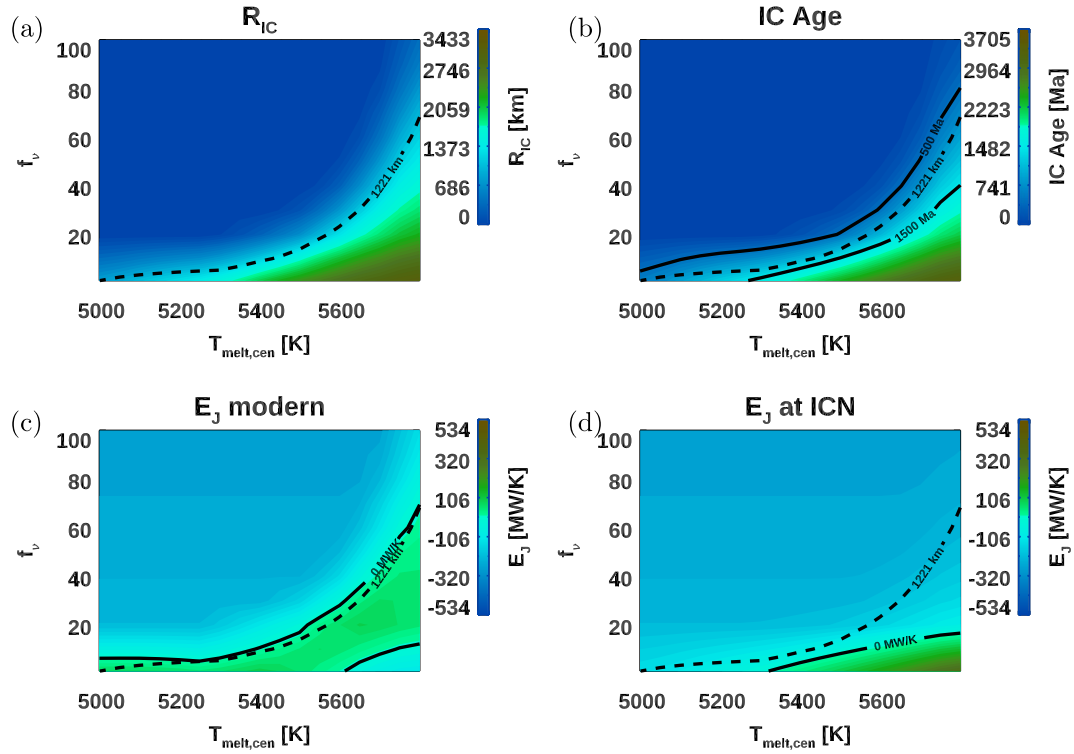

Figure 7. Parameter sweep over central core melting temperature $T_{melt,cen}$ and mantle viscosity ratio f_ν. Other control parameters are fixed to their nominal values: $k = 70$ Wm^{-1}K^{-1}, $Q_{c,rad} = 0$ TW, $Q_{m,rad} = 13$ TW, and $T_{cmb,0} = 4{,}570$ K. Contours of final inner core radius R_{IC} (a), age of inner core nucleation (b), core ohmic dissipation at the present-day E_J(4.5 Gyr) (c), and ohmic dissipation at inner core nucleation E_J(ICN) (d). In all contours Earth's present-day $R_{IC} = 1{,}221$ km is shown as a dashed black curve. Solid black lines denote inner core ages of 500 and 1,000 Ma in (b), and denote ohmic dissipation contours of 0 MW/K in (c) and (d). For reference, the nominal value of D15 is $T_{melt,cen} = 5{,}800$ K (corresponding to $T_{melt,ICB} = 5{,}500$ K).

4. Discussion

The thermal and magnetic history of the Earth is of great interest to many disciplines, and has seen a renaissance in recent years owing to upward revisions to the thermal conductivity of high P-T iron. In this paper we have coupled parameterized energy and entropy evolution models to explore the influence of six important control parameters: mantle viscosity ratio (f_ν), core thermal conductivity (k), core radiogenic heat rate ($Q_{c,rad}$), mantle radiogenic heating rate ($Q_{m,rad}$), central core melting temperature ($T_{melt,cen}$), and initial CMB temperature ($T_{cmb,0}$). A "successful" solution is one that produces the correct present-day inner core size is achieved and the dynamo is alive both prior to inner core nucleation and at the present-day, as is implied by the paleomagnetic record. An "unsuccessful" solution is one that produces either an incorrect present-day inner core radius, or no dynamo prior to inner core nucleation or at the present-day.

"Successful" solutions found with a low core thermal conductivity of 20 Wm^{-1}K^{-1} are unsatisfactory given the increasing number of studies that indicate the thermal conductivity is larger, perhaps by a factor of three or four. The new core paradox (Olson, 2013) is demonstrated by increasing the core thermal conductivity to 70 Wm^{-1}K^{-1}, which produces an unsuccessful solution where the dynamo is dead from 0.4 to 3.9 Gyr. Similarly, "successful" solutions that assume a high core radioactivity of 2.5 TW present-day (~340 ppm potassium) are unsatisfactory given the expected lithophilic nature of the main radiogenic elements (Blanchard et al., 2017; Bouhifd et al., 2007; Chidester et al., 2017, 2022; Corgne et al., 2007; Hirao et al., 2006; Watanabe et al., 2014; Xiong et al., 2018). A possible way out of this problem is to bury a "hidden reservoir" of radiogenic species in the LM (Jackson et al., 2010; Labrosse et al., 2007; Lee et al., 2010; Tolstikhin & Hofmann, 2005) instead of the core, although this hypothesis is highly debated (Campbell & O'Neill, 2012; Carlson et al., 2014; Jackson et al., 2014).

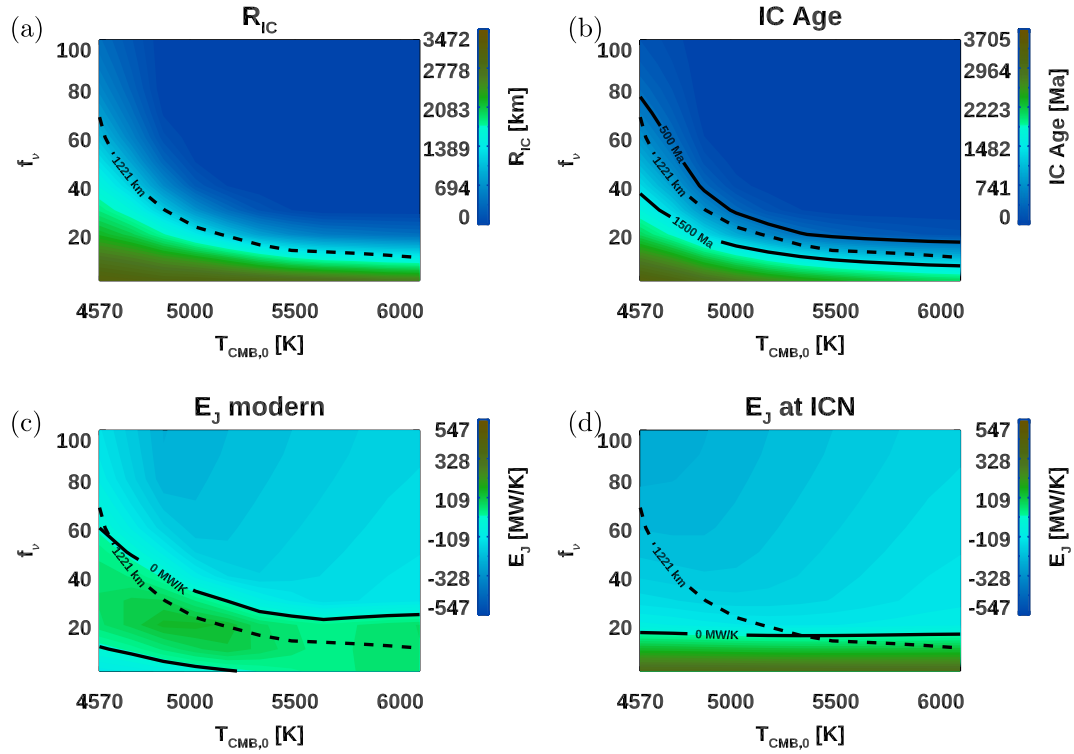

Figure 8. Parameter sweep over initial core-mantle boundary (CMB) temperature $T_{cmb,0}$ and mantle viscosity ratio f_ν. Other control parameters are fixed to their nominal values: $k = 70$ Wm^{-1}K^{-1}, $Q_{c,rad} = 0$ TW, $Q_{m,rad} = 13$ TW, and $T_{melt,cen} = 5{,}800$ K. Contours of final inner core radius R_{IC} (a), age of inner core nucleation (b), core ohmic dissipation at the present-day E_J(4.5 Gyr) (c), and ohmic dissipation at inner core nucleation E_J(ICN) (d). In all contours Earth's present-day $R_{IC} = 1{,}221$ km is shown as a dashed black curve. Solid black lines denote inner core ages of 500 and 1,000 Ma in (b), and denote ohmic dissipation contours of 0 MW/K in (c) and (d). For reference, the nominal initial CMB temperature of $T_{cmb,0} = 4{,}570$ K corresponds to an initial average core temperature of $T_{c,0} = 6{,}000$ K.

Perhaps the most promising solution we have found that assumes zero core radioactivity ($Q_{c,rad} = 0$ TW) and a reasonable thermal conductivity ($k = 70$ Wm^{-1}K^{-1}) is with a hot initial core temperature of $T_{cmb,0} \sim 6{,}000$ K, mantle viscosity ratio of $f_\nu = 5$, and low central melting temperature of $T_{melt,cen} = 5550$ K. In this particular model the inner core nucleates at ~630 Ma, grows to the correct final inner core radius, and achieves an ohmic dissipation rate at inner core nucleation that is very close to zero, implying the dynamo is marginal just prior inner core nucleation. A central melting temperature of 5,550 K corresponds to a melting temperature of ~5,200 K at the ICB, which is colder than most estimates but is within the range of 5,120 ± 390 K of Sinmyo et al. (2019). An initial CMB temperature of 6,000 K is higher than most estimates from core formation models (Fischer et al., 2017; King & Olson, 2011; Rubie et al., 2015), but given the lack of direct constraints on the initial thermal state of the core such a scenario should not be ruled out and deserves further scrutiny. The thermal evolution models of Labrosse (2015) and Nimmo (2015) also found that the dynamo can be kept alive with hot initial CMB temperatures without the need for core radioactivity.

One implication of such a hot initial CMB temperature is that the base of the mantle would be above its solidus, creating a BMO (Labrosse et al., 2007). The presence of a BMO could effect the rate of mantle and core cooling, possibly causing it to cool slower (Laneuville et al., 2018) or faster (Agrusta et al., 2020) depending on its composition and solidification style. Davies et al. (2020) finds that the presence of a long-lived BMO can modulate the CMB heat flow so that it is nearly constant, or even increasing over time, as the mantle cools. Davies and Greenwood (2021) coupled the mantle model of DB14 and the core model of Greenwood et al. (2021) to a modified version of the BMO model of Labrosse et al. (2007). In their successful solution (in the sense defined above), enhanced heat flow out of the BMO allowed magnetic field generation ($E_J > 0$) to begin around 4 Ga, while slow early cooling of the core due to latent heat release and radiogenic heating in

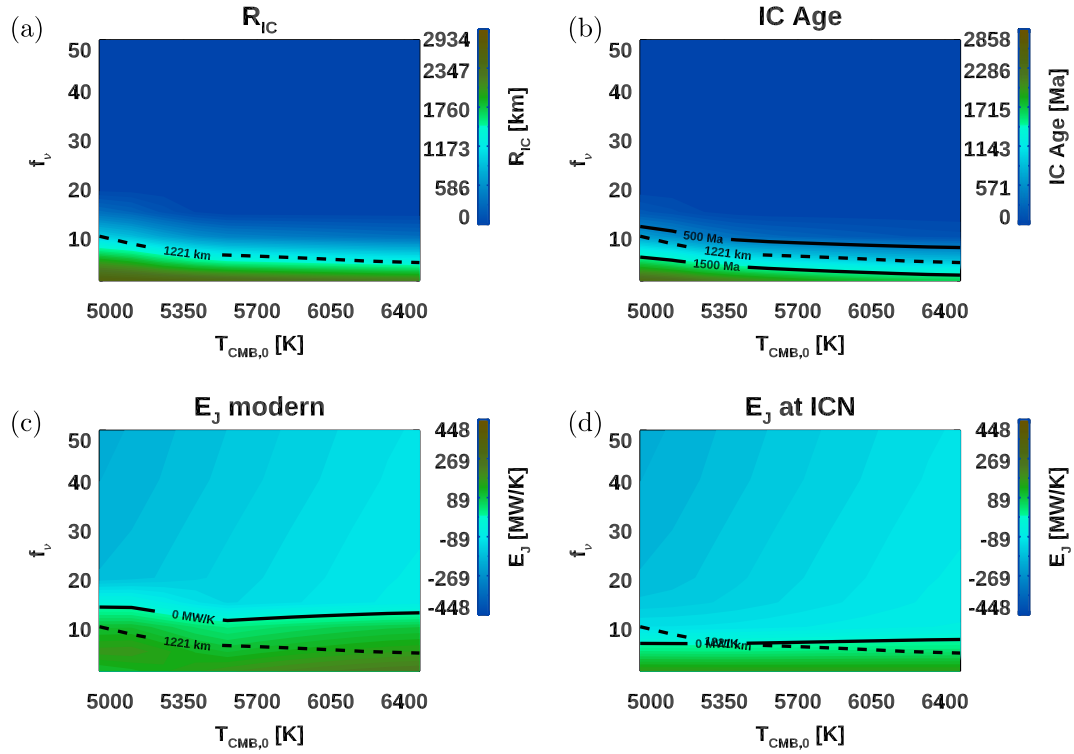

Figure 9. Parameter sweep over initial core-mantle boundary (CMB) temperature $T_{cmb,0}$ and mantle viscosity ratio f_ν with $T_{melt,cen}$ = 5,545 K ($T_{melt,330GPa}$ = 5,250 K). Other control parameters are fixed to their nominal values: k = 70 $Wm^{-1}K^{-1}$, $Q_{c,rad}$ = 0 TW, and $Q_{m,rad}$ = 13 TW. Contours of final inner core radius R_{IC} (a), age of inner core nucleation (b), core ohmic dissipation at the present-day E_J(4.5 Gyr) (c), and ohmic dissipation at inner core nucleation E_J(ICN) (d). In all contours Earth's present-day R_{IC} = 1,221 km is shown as a dashed black curve. Solid black lines denote inner core ages of 500 and 1,000 Ma in (b), and denote ohmic dissipation contours of 0 MW/K in (c) and (d). For reference, the nominal initial CMB temperature of $T_{cmb,0}$ = 4,570 K corresponds to an initial average core temperature of $T_{c,0}$ = 6,000 K.

the BMO kept the core hot such that E_J stayed above zero after the BMO completely freezes around 2.5 Ga. This solution used default parameters for the ICB density jump of 0.8 g/cc in Davies et al. (2015). Davies and Greenwood (2021) did not conduct an exhaustive parameter survey, but found that this successful solution does not exist for k > 70 W/m/K, in the absence of a BMO, or using the original BMO model of Labrosse et al. (2007). Future work should include a BMO and the parameter values suggested by our successful solution, which may open up a wider range of core histories that evade the new core paradox without recourse to radiogenic heating or precipitation.

In contrast to invoking a hot initial core, some studies have invoked the exact opposite: a cold initial mantle potential temperature, lower than the present day temperature of 1,630 K (Korenaga, 2006; O'Rourke et al., 2017; Patočka et al., 2020). These models integrate backward-in-time starting from estimates of the present-day mantle temperature and surface heat flow. Patočka et al. (2020) pointed out that such models can only yield a monotonic temperature history for a very specific radiogenic heat rate. This sensitivity is due to the non-linear nature of the thermal history equations, in particular the strong feedback between mantle viscosity and temperature. On the other hand, forward-in-time integrations are less sensitive to initial conditions but may not end with the expected final temperature and surface heat flow. Given the ~6% uncertainties in the present-day mantle temperature and surface heat flow (Jaupart et al., 2015), relying on these estimates to constrain an internal heating rate and initial mantle temperature carries significant uncertainties. Invoking an initially "cold" mantle conflicts with geochemical arguments that imply Earth's interior started "hot" following the Moon-forming giant impact (Carlson et al., 2014). Although, such a "cold" early state could still be plausible if the mantle cooled down rapidly to near present-day temperatures, and then heated back up due to radiogenic heat.

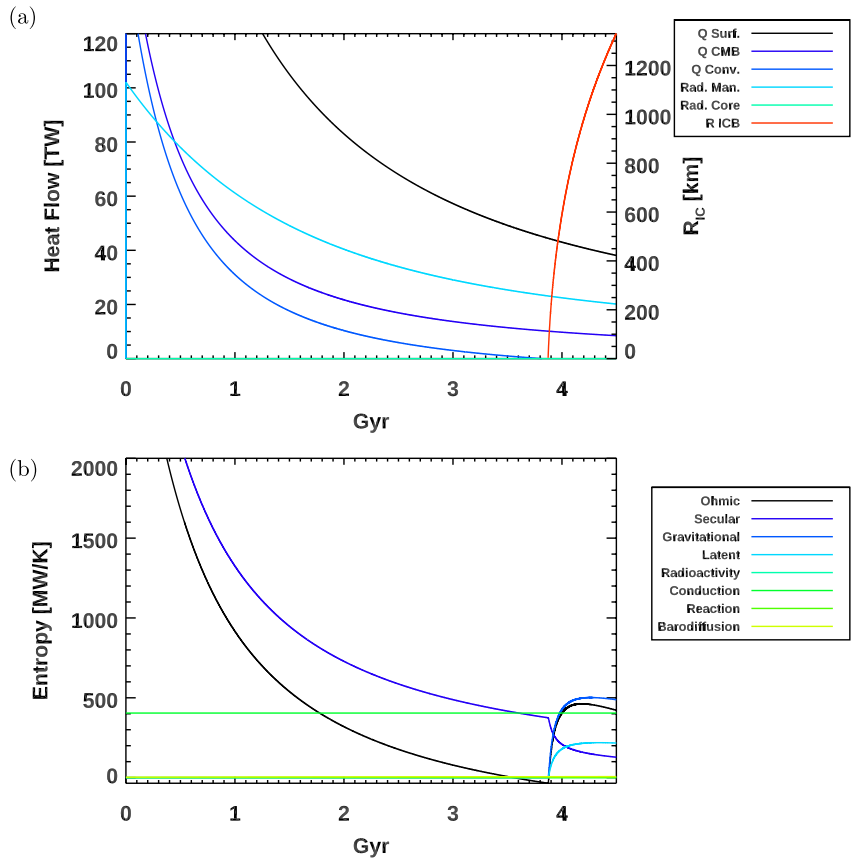

Figure 10. A "successful" thermal evolution model with $k = 70$ Wm^{-1}K^{-1}, $f_\nu = 5$, $T_{cmb,0} = 6{,}015$ K ($T_{c,0} = 7{,}900$ K), $T_{melt,cen} = 5{,}545$ K ($T_{melt,330\text{GPa}} = 5{,}250$ K), $Q_{c,rad} = 0$ TW, $Q_{m,rad} = 13$ TW, which produces an inner core age of 627 Ma. (a) Heat flows at the surface, core-mantle boundary (CMB), CMB minus core adiabat (i.e., core convective), mantle and core radioactivity, and at the inner core boundary. Inner core radius R_{IC} (red) is shown on right y-axis. (b) Entropy evolution of the same model.

Appendix A: Thermal Evolution Model Details

This appendix describes some details of the mantle thermal evolution model used above. The interested reader is referred to Driscoll and Bercovici (2014) for more detail. The mantle surface heat flow Q_{surf} is limited by heat conduction through the UM thermal boundary layer, which can be approximated by

$$Q_{surf} = Ak_{UM}\frac{\Delta T_{UM}}{\delta_{UM}} \tag{A1}$$

where $\Delta T_{UM} = T_{UM} - T_g$ is the temperature jump across the UM thermal boundary layer δ_{UM}, A is surface area, and $k_{UM} = 4.2$ Wm^{-1}K^{-1} is UM thermal conductivity. δ_{UM} is derived by assuming that the Rayleigh number of the boundary layer Ra_{UM} be equal to the critical Rayleigh number for thermal convection $Ra_c \approx 660$. At the base of the thermal boundary layer,

$$Ra_{UM} = \frac{\alpha g \Delta T_{UM}\delta_{UM}^3}{\kappa \nu_{UM}} \tag{A2}$$

where $\alpha = 3 \times 10^{-5}$ K^{-1} is thermal expansivity, $g = 9.8$ ms^{-2} is gravity, $\kappa = 1 \times 10^{-6}$ m^{2}s^{-1} is thermal diffusivity, and ν_{UM} is boundary layer viscosity. Mantle viscosity is assumed to follow an Arrhenius law,

$$\nu_m(T) = \nu_0 \exp\left[\frac{A_\nu}{R_g T_m}\right] \tag{A3}$$

where $\nu_0 = 7 \times 10^7$ m^{2}s^{-1} is a reference viscosity, $A_\nu = 3 \times 10^5$ Jmol^{-1} is the activation energy, and R_g is the gas constant. The upper-mantle viscosity ν_{UM} is assumed to be smaller than ν_m by a factor of 10, and the ratio of LM to UM viscosity $f_\nu = \nu_{LM}/\nu_{UM}$ is varied over a wide range (1–100) in the models above. Combining Equations A2 and A1 gives,

$$Q_{surf} = Ak_{UM}\left(\frac{\alpha g}{Ra_c \kappa \nu_{UM}}\right)^{1/3}(\eta_{UM}\Delta T_m)^{4/3} \tag{A4}$$

where the thermal boundary layer temperature jump ΔT_{UM} has been replaced by $\Delta T_{UM} \approx \eta_{UM}\Delta T_m$, where $\eta_{UM} = \exp(-(R_{UM} - R_m)\alpha g/c_p) \approx 0.7$ is the adiabatic temperature decrease from the average mantle temperature to the bottom of the UM thermal boundary layer, and $\Delta T_m = T_m - T_g$.

Data Availability Statement

All data and plotting scripts are available at https://osf.io/jczhe/.

Acknowledgments
We thank S. Labrosse and K. Ohta for thorough and helpful reviews.

References

Adeleke, A. A., & Yao, Y. (2020). Formation of stable compounds of potassium and iron under pressure. *The Journal of Physical Chemistry A*, *124*(23), 4752–4763. https://doi.org/10.1021/acs.jpca.0c03330

Agrusta, R., Morison, A., Labrosse, S., Deguen, R., Alboussière, T., Tackley, P., & Dubuffet, F. (2020). Mantle convection interacting with magma oceans. *Geophysical Journal International*, *220*(3), 1878–1892. https://doi.org/10.1093/gji/ggz549

Andrault, D., Monteux, J., Le Bars, M., & Samuel, H. (2016). The deep Earth may not be cooling down. *Earth and Planetary Science Letters*, *443*, 195–203. https://doi.org/10.1016/j.epsl.2016.03.020

Arevalo, R., McDonough, W. F., & Luong, M. (2009). The K/U ratio of the silicate Earth: Insights into mantle composition, structure and thermal evolution. *Earth and Planetary Science Letters*, *278*(3), 361–369. https://doi.org/10.1016/j.epsl.2008.12.023

Badro, J., Aubert, J., Hirose, K., Nomura, R., Blanchard, I., Borensztajn, S., & Siebert, J. (2018). Magnesium partitioning between Earth's mantle and core and its potential to drive an early exsolution geodynamo. *Geophysical Research Letters*, *45*(24), 13240–13248. https://doi.org/10.1029/2018gl080405

Basu, A., Field, M. R., McCulloch, D. G., & Boehler, R. (2020). New measurement of melting and thermal conductivity of iron close to outer core conditions. *Geoscience Frontiers*, *11*(2), 565–568. (Grain Crushing in Geoscience Materials). https://doi.org/10.1016/j.gsf.2019.06.007

Biggin, A. J., Bono, R. K., Meduri, D. G., Sprain, C. J., Davies, C. J., Holme, R., & Doubrovine, P. V. (2020). Quantitative estimates of average geomagnetic axial dipole dominance in deep geological time. *Nature Communications*, *11*(1), 1–9. https://doi.org/10.1038/s41467-020-19794-7

Blanchard, I., Siebert, J., Borensztajn, S., & Badro, J. (2017). The solubility of heat-producing elements in Earth's core. *Geochemical Perspectives Letters*, *5*, 1–5. https://doi.org/10.7185/geochemlet.1737

Bono, R. K., Paterson, G. A., van der Boon, A., Engbers, Y. A., Michael Grappone, J., Handford, B., et al. (2022). The pint database: A definitive compilation of absolute palaeomagnetic intensity determinations since 4 billion years ago. *Geophysical Journal International*, *229*(1), 522–545. https://doi.org/10.1093/gji/ggab490

Bouhifd, M., Gautron, L., Bolfan-Casanova, N., Malavergne, V., Hammouda, T., Andrault, D., & Jephcoat, A. (2007). Potassium partitioning into molten iron alloys at high-pressure: Implications for Earth's core. *Physics of the Earth and Planetary Interiors*, *160*(1), 22–33. https://doi.org/10.1016/j.pepi.2006.08.005

Boyet, M., & Carlson, R. W. (2006). A new geochemical model for the Earth's mantle inferred from 146Sm–142Nd systematics. *Earth and Planetary Science Letters*, *250*(1–2), 254–268. https://doi.org/10.1016/j.epsl.2006.07.046

Campbell, I. H., & O'Neill, H. S. C. (2012). Evidence against a chondritic Earth. *Nature*, *483*(7391), 553–558. https://doi.org/10.1038/nature10901

Carlson, R. W., Garnero, E., Harrison, T. M., Li, J., Manga, M., McDonough, W. F., et al. (2014). How did early Earth become our modern world? *Annual Review of Earth and Planetary Sciences*, *42*(1), 151–178. https://doi.org/10.1146/annurev-earth-060313-055016

Chidester, B. A., Lock, S., Swadba, K., Rahman, Z., Righter, K., & Campbell, A. J. (2022). The lithophile element budget of Earth's core. *Geochemistry, Geophysics, Geosystems*, *23*(2), e2021GC009986. https://doi.org/10.1029/2021gc009986

Chidester, B. A., Rahman, Z., Righter, K., & Campbell, A. J. (2017). Metal–silicate partitioning of U: Implications for the heat budget of the core and evidence for reduced U in the mantle. *Geochimica et Cosmochimica Acta*, *199*, 1–12. https://doi.org/10.1016/j.gca.2016.11.035

Christensen, U. (1985). Thermal evolution models for the Earth. *Journal of Geophysical Research*, *90*(B4), 2995–3007. https://doi.org/10.1029/jb090ib04p02995

Christensen, U. (2018). Geodynamo models with a stable layer and heterogeneous heat flow at the top of the core. *Geophysical Journal International*, *215*(2), 1338–1351. https://doi.org/10.1093/gji/ggy352

Conrad, C. P., & Hager, B. H. (1999). The thermal evolution of an Earth with strong subduction zones. *Geophysical Research Letters*, *26*(19), 3041–3044. https://doi.org/10.1029/1999gl005397

Corgne, A., Keshav, S., Fei, Y., & McDonough, W. F. (2007). How much potassium is in the Earth's core? New insights from partitioning experiments. *Earth and Planetary Science Letters*, *256*(3), 567–576. https://doi.org/10.1016/j.epsl.2007.02.012

Davies, C., & Greenwood, S. (2021). Core-mantle coevolution—A multidisciplinary approach. In *(chap. Dynamics in Earth's core arising from thermo-chemical interactions with the mantle)*. Wiley.

Davies, C., Pozzo, M., Gubbins, D., & Alfè, D. (2015). Constraints from material properties on the dynamics and evolution of Earth's core. *Nature Geoscience*, *8*(9), 678–685. https://doi.org/10.1038/ngeo2492

Davies, C. J. (2015). Cooling history of Earth's core with high thermal conductivity. *Physics of the Earth and Planetary Interiors*, *247*, 65–79. https://doi.org/10.1016/j.pepi.2015.03.007

Davies, C. J., Pozzo, M., Gubbins, D., & Alfè, D. (2020). Transfer of oxygen to Earth's core from a long-lived magma ocean. *Earth and Planetary Science Letters*, *538*, 116208. https://doi.org/10.1016/j.epsl.2020.116208

Davies, G. (1980). Thermal histories of convective Earth models and constraints on radiogenic heat production in the Earth. *Journal of Geophysical Research*, *85*(B5), 2517. https://doi.org/10.1029/jb085ib05p02517

Davies, G. (2007). Mantle regulation of core cooling: A geodynamo without core radioactivity? *Physics of the Earth and Planetary Interiors*, *160*(3–4), 215–229. https://doi.org/10.1016/j.pepi.2006.11.001

Davies, G. (2009). Effect of plate bending on the Urey ratio and the thermal evolution of the mantle. *Earth and Planetary Science Letters*, *287*(3), 513–518. https://doi.org/10.1016/j.epsl.2009.08.038

de Koker, N., Steinle-Neumann, G., & Vlček, V. (2012). Electrical resistivity and thermal conductivity of liquid Fe alloys at high P and T, and heat flux in Earth's core. *Proceedings of the National Academy of Sciences of United States of America*, *109*(11), 4070–4073. https://doi.org/10.1073/pnas.1111841109

Deng, J., & Lee, K. K. (2017). Viscosity jump in the lower mantle inferred from melting curves of ferropericlase. *Nature Communications*, *8*(1), 1–8. https://doi.org/10.1038/s41467-017-02263-z

Driscoll, P., & Bercovici, D. (2014). On the thermal and magnetic histories of Earth and Venus: Influences of melting, radioactivity, and conductivity. *Physics of the Earth and Planetary Interiors*, *236*, 36–51. https://doi.org/10.1016/j.pepi.2014.08.004

Du, Z., Boujibar, A., Driscoll, P., & Fei, Y. (2019). Experimental constraints on an MgO exsolution-driven geodynamo. *Geophysical Research Letters*, *46*(13), 7379–7385. https://doi.org/10.1029/2019GL083017

Du, Z., Jackson, C., Bennett, N., Driscoll, P., Deng, J., Lee, K. K., et al. (2017). Insufficient energy from MgO exsolution to power early geodynamo. *Geophysical Research Letters*, *44*(22), 11376–11381. https://doi.org/10.1002/2017gl075283

Faure, P., Bouhifd, M., Boyet, M., Manthilake, G., Clesi, V., & Devidal, J.-L. (2020). Uranium and thorium partitioning in the bulk silicate Earth and the oxygen content of Earth's core. *Geochimica et Cosmochimica Acta*, *275*, 83–98. https://doi.org/10.1016/j.gca.2020.02.010

Fischer, R. A., Campbell, A. J., & Ciesla, F. J. (2017). Sensitivities of Earth's core and mantle compositions to accretion and differentiation processes. *Earth and Planetary Science Letters*, *458*, 252–262. https://doi.org/10.1016/j.epsl.2016.10.025

Fu, R. R., Drabon, N., Wiedenbeck, M., Brenner, A. R., Lowe, D. R., & Borlina, C. S. (2021). Paleomagnetism of 3.5-4.0 Ga zircons from the Barberton greenstone belt, South Africa. *Earth and Planetary Science Letters*, *567*, 116999. https://doi.org/10.1016/j.epsl.2021.116999

Gando, A., Dwyer, D., McKeown, R., & Zhang, C. (2011). Partial radiogenic heat model for Earth revealed by geoneutrino measurements. *Nature Geoscience*, *4*(9), 647–651. https://doi.org/10.1038/ngeo1205

Gastine, T., Aubert, J., & Fournier, A. (2020). Dynamo-based limit to the extent of a stable layer atop Earth's core. *Geophysical Journal International*, *222*(2), 1433–1448. https://doi.org/10.1093/gji/ggaa250

Gerardi, G., Ribe, N. M., & Tackley, P. J. (2019). Plate bending, energetics of subduction and modeling of mantle convection: A boundary element approach. *Earth and Planetary Science Letters*, *515*, 47–57. https://doi.org/10.1016/j.epsl.2019.03.010

Gomi, H., Ohta, K., Hirose, K., Labrosse, S., Caracas, R., Verstraete, M. J., & Hernlund, J. W. (2013). The high conductivity of iron and thermal evolution of the Earth's core. *Physics of the Earth and Planetary Interiors*, *224*, 88–103. https://doi.org/10.1016/j.pepi.2013.07.010

Greenwood, S., Davies, C. J., & Mound, J. E. (2021). On the evolution of thermally stratified layers at the top of Earth's core. *Physics of the Earth and Planetary Interiors*, *318*, 106763. https://doi.org/10.1016/j.pepi.2021.106763

Gubbins, D., Alfe, D., Masters, G., Price, G., & Gillan, M. (2003). Can the Earth's dynamo run on heat alone? *Geophysical Journal International*, *155*(2), 609–622. https://doi.org/10.1046/j.1365-246x.2003.02064.x

Gubbins, D., Alfe, D., Masters, G., Price, G., & Gillan, M. (2004). Gross thermodynamics of two-component core convection. *Geophysical Journal International*, *157*(3), 1407–1414. https://doi.org/10.1111/j.1365-246x.2004.02219.x

Helffrich, G., & Kaneshima, S. (2010). Outer-core compositional stratification from observed core wave speed profiles. *Nature*, *468*(7325), 807–810. https://doi.org/10.1038/nature09636

Herzberg, C., Condie, K., & Korenaga, J. (2010). Thermal history of the Earth and its petrological expression. *Earth and Planetary Science Letters*, *292*(1–2), 79–88. https://doi.org/10.1016/j.epsl.2010.01.022

Hirao, N., Ohtani, E., Kondo, T., Endo, N., Kuba, T., Suzuki, T., & Kikegawa, T. (2006). Partitioning of potassium between iron and silicate at the core-mantle boundary. *Geophysical Research Letters*, *33*(8), L08303. https://doi.org/10.1029/2005gl025324

Hirose, K., Morard, G., Sinmyo, R., Umemoto, K., Hernlund, J., Helffrich, G., & Labrosse, S. (2017). Crystallization of silicon dioxide and compositional evolution of the Earth's core. *Nature*, *543*(7643), 99–102. https://doi.org/10.1038/nature21367

Hirose, K., Wood, B., & Vočadlo, L. (2021). Light elements in the Earth's core. *Nature Reviews Earth & Environment*, *2*(9), 645–658. https://doi.org/10.1038/s43017-021-00203-6

Hsieh, W.-P., Goncharov, A. F., Labrosse, S., Holtgrewe, N., Lobanov, S. S., Chuvashova, I., et al. (2020). Low thermal conductivity of iron-silicon alloys at Earth's core conditions with implications for the geodynamo. *Nature Communications*, *11*(1), 3332. https://doi.org/10.1038/s41467-020-17106-7

Inoue, H., Suehiro, S., Ohta, K., Hirose, K., & Ohishi, Y. (2020). Resistivity saturation of hcp Fe-Si alloys in an internally heated diamond anvil cell: A key to assessing the Earth's core conductivity. *Earth and Planetary Science Letters*, *543*, 116357. https://doi.org/10.1016/j.epsl.2020.116357

Jackson, C. R., Ziegler, L. B., Zhang, H., Jackson, M. G., & Stegman, D. R. (2014). A geochemical evaluation of potential magma ocean dynamics using a parameterized model for perovskite crystallization. *Earth and Planetary Science Letters*, *392*, 154–165. https://doi.org/10.1016/j.epsl.2014.01.028

Jackson, M. G., Carlson, R. W., Kurz, M. D., Kempton, P. D., Francis, D., & Blusztajn, J. (2010). Evidence for the survival of the oldest terrestrial mantle reservoir. *Nature*, *466*(7308), 853–856. https://doi.org/10.1038/nature09287

Jaupart, C., Labrosse, S., Lucazeau, F., & Mareschal, J. C. (2015). Temperatures, heat, and energy in the mantle of the Earth. In D. Bercovici (Ed.), *Treatise on geophysics*, *Mantle dynamics* (2nd ed., Vol. 7, pp. 253–305). Elsevier.

Keller, B., & Schoene, B. (2018). Plate tectonics and continental basaltic geochemistry throughout Earth history. *Earth and Planetary Science Letters*, *481*, 290–304. https://doi.org/10.1016/j.epsl.2017.10.031

King, C., & Olson, P. (2011). Heat partitioning in metal-silicate plumes during Earth differentiation. *Earth and Planetary Science Letters*, *304*(3), 577–586. https://doi.org/10.1016/j.epsl.2011.02.037

Konôpková, Z., McWilliams, R. S., Gómez-Pérez, N., & Goncharov, A. F. (2016). Direct measurement of thermal conductivity in solid iron at planetary core conditions. *Nature*, *534*(7605), 99–101. https://doi.org/10.1038/nature18009

Korenaga, J. (2006). Archean geodynamics and the thermal evolution of Earth. *Geophysical Monograph-American Geophysical Union*, *164*, 7–32.

Labrosse, S. (2015). Thermal evolution of the core with a high thermal conductivity. *Physics of the Earth and Planetary Interiors*, *247*, 36–55. https://doi.org/10.1016/j.pepi.2015.02.002

Labrosse, S., Hernlund, J., & Coltice, N. (2007). A crystallizing dense magma ocean at the base of the Earth's mantle. *Nature*, *450*(7171), 866–869. https://doi.org/10.1038/nature06355

Labrosse, S., Morison, A., Deguen, R., & Alboussière, T. (2018). Rayleigh–Bénard convection in a creeping solid with melting and freezing at either or both its horizontal boundaries. *Journal of Fluid Mechanics*, *846*, 5–36. https://doi.org/10.1017/jfm.2018.258

Landeau, M., Fournier, A., Nataf, H.-C., Cébron, D., & Schaeffer, N. (2022). *Sustaining earth's magnetic dynamo*. Nature Reviews Earth & Environment.

Laneuville, M., Hernlund, J., Labrosse, S., & Guttenberg, N. (2018). Crystallization of a compositionally stratified basal magma ocean. *Physics of the Earth and Planetary Interiors*, *276*, 86–92. https://doi.org/10.1016/j.pepi.2017.07.007

Lee, C.-T. A., Luffi, P., Höink, T., Li, J., Dasgupta, R., & Hernlund, J. (2010). Upside-down differentiation and generation of a "primordial" lower mantle. *Nature*, *463*(7283), 930–933. https://doi.org/10.1038/nature08824

Li, W.-J., Li, Z., He, X.-T., Wang, C., & Zhang, P. (2021). Constraints on the thermal evolution of Earth's core from ab initio calculated transport properties of FeNi liquids. *Earth and Planetary Science Letters*, *562*, 116852. https://doi.org/10.1016/j.epsl.2021.116852

Marquardt, H., & Miyagi, L. (2015). Slab stagnation in the shallow lower mantle linked to an increase in mantle viscosity. *Nature Geoscience*, *8*(4), 311–314.

Mittal, T., Knezek, N., Arveson, S. M., McGuire, C. P., Williams, C. D., Jones, T. D., & Li, J. (2020). Precipitation of multiple light elements to power Earth's early dynamo. *Earth and Planetary Science Letters*, *532*, 116030. https://doi.org/10.1016/j.epsl.2019.116030

Monteux, J., Andrault, D., & Samuel, H. (2016). On the cooling of a deep terrestrial magma ocean. *Earth and Planetary Science Letters*, *448*, 140–149. https://doi.org/10.1016/j.epsl.2016.05.010

Nimmo, F. (2015). 8.02—Energetics of the core. In G. Schubert (Ed.), *Treatise on geophysics* (2nd ed., pp. 27–55). Elsevier.

Nimmo, F., Price, G., Brodholt, J., & Gubbins, D. (2004). The influence of potassium on core and geodynamo evolution. *Geophysical Journal International*, *156*(2), 363–376. https://doi.org/10.1111/j.1365-246x.2003.02157.x

Olson, P. (2013). The new core paradox. *Science*, *342*(6157), 431–432. https://doi.org/10.1126/science.1243477

Olson, P., Landeau, M., & Hirsh, B. H. (2017). Laboratory experiments on rain-driven convection: Implications for planetary dynamos. *Earth and Planetary Science Letters*, *457*, 403–411. https://doi.org/10.1016/j.epsl.2016.10.015

O'Rourke, J. G., Korenaga, J., & Stevenson, D. J. (2017). Thermal evolution of Earth with magnesium precipitation in the core. *Earth and Planetary Science Letters*, *458*, 263–272. https://doi.org/10.1016/j.epsl.2016.10.057

O'Rourke, J. G., & Stevenson, D. J. (2016). Powering Earth's dynamo with magnesium precipitation from the core. *Nature*, *529*(7586), 387–389. https://doi.org/10.1038/nature16495

Patočka, V., Šrámek, O., & Tosi, N. (2020). Minimum heat flow from the core and thermal evolution of the Earth. *Physics of the Earth and Planetary Interiors*, *305*, 106457. https://doi.org/10.1016/j.pepi.2020.106457

Pozzo, M., Davies, C., Gubbins, D., & Alfè, D. (2012). Thermal and electrical conductivity of iron at Earth's core conditions. *Nature*, *485*(7398), 355–358. https://doi.org/10.1038/nature11031

Pozzo, M., Davies, C. J., & Alfè, D. (2022). Towards reconciling experimental and computational determinations of Earth's core thermal conductivity. *Earth and Planetary Science Letters*, *584*, 117466. https://doi.org/10.1016/j.epsl.2022.117466

Rubie, D. C., Jacobson, S. A., Morbidelli, A., O'Brien, D. P., Young, E. D., de Vries, J., et al. (2015). Accretion and differentiation of the terrestrial planets with implications for the compositions of early-formed solar system bodies and accretion of water. *Icarus*, *248*, 89–108. https://doi.org/10.1016/j.icarus.2014.10.015

Saha, P., Mazumder, A., & Mukherjee, G. D. (2020). Thermal conductivity of dense hcp iron: Direct measurements using laser heated diamond anvil cell. *Geoscience Frontiers*, *11*(5), 1755–1761. https://doi.org/10.1016/j.gsf.2019.12.010

Sammon, L. G., & McDonough, W. F. (2022). Quantifying Earth's radiogenic heat budget. *Earth and Planetary Science Letters*, *593*, 117684. https://doi.org/10.1016/j.epsl.2022.117684

Sinmyo, R., Hirose, K., & Ohishi, Y. (2019). Melting curve of iron to 290 GPa determined in a resistance-heated diamond-anvil cell. *Earth and Planetary Science Letters*, *510*, 45–52. https://doi.org/10.1016/j.epsl.2019.01.006

Stacey, F., & Anderson, O. L. (2001). Electrical and thermal conductivities of Fe-Ni-Si alloy under core conditions. *Physics of the Earth and Planetary Interiors*, *124*(3–4), 153–162. https://doi.org/10.1016/s0031-9201(01)00186-8

Stacey, F., & Loper, D. (2007). A revised estimate of the conductivity of iron alloy at high pressure and implications for the core energy balance. *Physics of the Earth and Planetary Interiors*, *161*(1–2), 13–18. https://doi.org/10.1016/j.pepi.2006.12.001

Tarduno, J. A., Cottrell, R. D., Bono, R. K., Oda, H., Davis, W. J., Fayek, M., et al. (2020). Paleomagnetism indicates that primary magnetite in zircon records a strong Hadean geodynamo. *Proceedings of the National Academy of Sciences of United States of America*, *117*(5), 2309–2318. https://doi.org/10.1073/pnas.1916553117

Tauxe, L., & Yamazaki, T. (2015). 5.13—Paleointensities. In G. Schubert (Ed.), *Treatise on geophysics* (2nd ed., pp. 461–509). Elsevier.

Tolstikhin, I., & Hofmann, A. W. (2005). Early crust on top of the Earth's core. *Physics of the Earth and Planetary Interiors*, *148*(2), 109–130. https://doi.org/10.1016/j.pepi.2004.05.011

Watanabe, K., Ohtani, E., Kamada, S., Sakamaki, T., Miyahara, M., & Ito, Y. (2014). The abundance of potassium in the Earth's core. *Physics of the Earth and Planetary Interiors*, *237*, 65–72. https://doi.org/10.1016/j.pepi.2014.10.001

Williams, Q. (2018). The thermal conductivity of Earth's core: A key geophysical parameter's constraints and uncertainties. *Annual Review of Earth and Planetary Sciences*, *46*(1), 47–66. https://doi.org/10.1146/annurev-earth-082517-010154

Wohlers, A., & Wood, B. J. (2015). A mercury-like component of early Earth yields uranium in the core and high mantle 142nd. *Nature*, *520*(7547), 337–340. https://doi.org/10.1038/nature14350

Xiong, Z., Tsuchiya, T., & Taniuchi, T. (2018). Ab initio prediction of potassium partitioning into Earth's core. *Journal of Geophysical Research: Solid Earth*, *123*(8), 6451–6458. https://doi.org/10.1029/2018jb015522

Xu, J., Zhang, P., Haule, K., Minar, J., Wimmer, S., Ebert, H., & Cohen, R. E. (2018). Thermal conductivity and electrical resistivity of solid iron at Earth's core conditions from first principles. *Physical Review Letters*, *121*(9), 096601. https://doi.org/10.1103/PhysRevLett.121.096601

Zhang, Y., Hou, M., Liu, G., Zhang, C., Prakapenka, V. B., Greenberg, E., et al. (2020). Reconciliation of experiments and theory on transport properties of iron and the geodynamo. *Physical Review Letters*, *125*(7), 078501. https://doi.org/10.1103/physrevlett.125.078501

Zhang, Y., Luo, K., Hou, M., Driscoll, P., Salke, N. P., Minár, J., et al. (2022). Thermal conductivity of Fe-Si alloys and thermal stratification in Earth's core. *Proceedings of the National Academy of Sciences of United States of America*, *119*(1). https://doi.org/10.1073/pnas.2119001119